# Optically induced angular alignment of trapped birefringent micro-objects by linearly polarized light

E. Higurashi,* R. Sawada, and T. Ito
*NTT Opto-electronics Laboratories, 3-9-11 Midori-cho, Musashino-shi, Tokyo 180-8585, Japan*
(Received 20 July 1998; revised manuscript received 7 December 1998)

Optically induced mechanical angular alignment of trapped birefringent micrometer-sized objects resulting from the transfer of angular momentum produced by birefringence using linearly polarized light has been experimentally demonstrated. Fluorinated polyimide (PMDA/TFDB) micro-objects having a large birefringence of $\Delta n = n_{slow} - n_{fast} = 0.13$ (refractive indices $n_{slow} = 1.62$, $n_{fast} = 1.49$), which were fabricated by micromachining (reactive ion etching) and suspended in water ($n = 1.33$), were trapped and manipulated by radiation pressure from a single focused Gaussian beam (wavelength $\lambda = 1.064$ $\mu$m, power $> 130$ $\mu$W). The effect of the linearly polarized light on such micro-objects showed that they were angularly aligned about the laser beam axis and their angular position could be smoothly controlled by rotating the vibration plane of the electric field. We have shown that the retardation of the birefringent micro-object determines which axis (fast or slow) of the micro-object coincides with the vibration plane of the electric field of the incident light.
[S1063-651X(99)09603-8]

PACS number(s): 42.62.−b, 42.88.+h, 42.50.Vk, 42.50.Ct

Optical manipulation of microscopic particles by radiation pressure [1,2] has become a powerful tool for use as optical tweezers by researchers in many fields, including biology, physics, and chemistry [3]. Recently, this manipulative capability has been extended from merely confining, transporting, and patterning particles to also rotating them. For example, optically induced rotation of micromachined objects has been demonstrated for creating radiation-pressure-driven micromotors for micromechanical systems [4,5]. The optical torque arises from the radiation pressure exerted on the object's sidewalls and has been analyzed using a ray-optics model [6,7]. Some advanced studies related to improving the design of the objects' shape have also been reported [8–11]. This optically induced rotation has the advantage of not requiring direct contact or electrical wires for power supply. Nevertheless, the micro-objects cannot be held at specific angles, because this type of rotation is continuous. Mechanical angular alignment is another requirement for the assembly of microcomponents for fabrication of three-dimensional structures or alignment of micro-optical components in micro-opto-mechanical systems applications.

Light-induced continuous rotation of optically trapped absorbing particles resulting from the transfer of spin [12] or orbital [13] angular momentum has been observed [14–21] and calculated [22–24]. Recently, angular alignment of optically trapped birefringent micro-objects with a linearly polarized laser beam has been observed [25,26]. Here, we combined micromachining and a processable polymer material having a large birefringence to fabricate the shape-controlled birefringent micro-objects with a known location of the optic axis. We experimentally demonstrate angular alignment resulting from the transfer of angular momentum due to the photon spin produced by birefringence to the trapped birefringent micro-object when using linearly polarized light. We show that the retardation of the birefringent micro-object determines which axis (fast or slow) of the micro-object coincides with the vibration plane of the electric field of the incident light.

In addition, changing the state of polarization from linear to circular caused continuous rotation of the trapped birefringent micro-objects due to spin angular momentum. Since Beth's first experimental observation of the torque on a macroscopic wave plate suspended from a fiber [12], numerous experiments to detect this extremely small radiation torque have been demonstrated or proposed [27–29]. Our results clearly show that the effect of continuous rotation on optically trapped transparent birefringent micro-objects is relatively easy to observe.

Figure 1 shows how we used a linearly polarized laser beam to angularly align an optically trapped birefringent micro-object in water. The incident light is in the circularly symmetric Gaussian mode, linearly polarized, and directed opposite to the $z$ direction. We consider the central portion of the Gaussian beam, i.e., this portion can be assumed to be a collimated (parallel) beam and is incident normally to the micro-object. The micro-object (Mie particle) under consideration is made of transparent birefringent material (birefringence $\Delta n = n_{slow} - n_{fast}$). In the ($x$-$y$) plane (top view) the micro-object has the shape of a square, as shown in Fig. 1(a), and flat surfaces on the top, bottom, and sides (thickness $= d$). Here the birefringent micro-object is a negative uniaxial crystal with its fast (optic) and slow axes perpendicular to the $z$ axis. Consider, for example, the case where the retardation $R(\Delta n \times d)$ produced by the birefringent micro-object is in the range of $0 < R < \lambda/2$ ($\lambda$: wavelength).

In Fig. 1(b), the slow axis of the birefringent micro-object makes an angle of $\theta$ with respect to the vibration plane of the incident electric field ($x$ axis). When linearly polarized light with zero angular momentum is transmitted through the birefringent micro-object, the transmitted light generally becomes right elliptically polarized light (rotating clockwise in

*Electronic address: eiji@ilab.ntt.co.jp

 

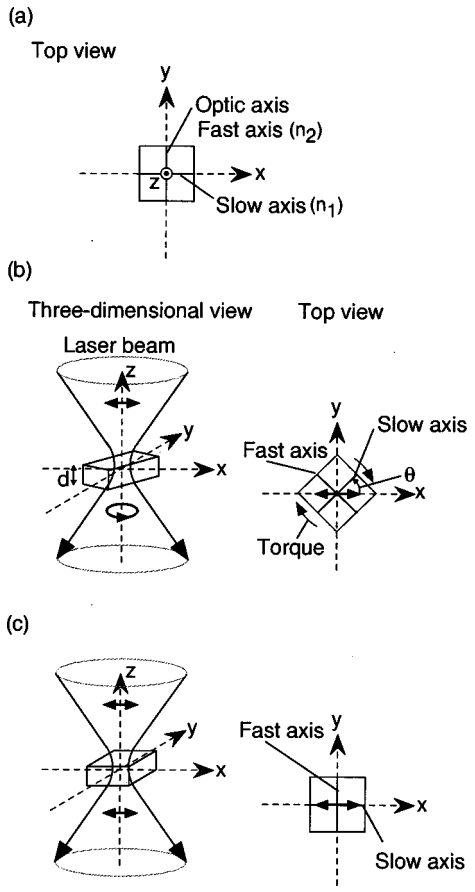


FIG. 1. Schematic illustrating how a trapped birefringent micro-object was angularly aligned using a linearly polarized laser beam. (a) Top view of the birefringent micro-object. Retardation $R$ of the birefringent micro-object was assumed to be $0<R<\lambda/2$ for the collimated light. The micro-object was immersed in water. (b) Three-dimensional view of optical trapping on the left and top view of the micro-object on the right with the state of polarization. The slow axis of the micro-object made an angle $\theta$ with respect to the vibration plane of the incident electric field vector ($x$ axis). (c) The slow axis became coincident with the vibration plane of the electric field vector.

a fixed plane as viewed facing into the light) carrying angular momentum. That is, the interaction of light with the micro-object results in a change in photon angular momentum through the process of transmission. As a result of the conservation of angular momentum, the micro-object gains angular momentum and experiences a corresponding torque about the $z$ axis in the direction opposite to the resultant elliptically polarized light. In response to the radiation torque, the micro-object rotates and its slow axis becomes coincident with the vibration plane of the electric field [Fig. 1(c)]. Now, the birefringent micro-object no longer changes the state of polarization (linear) of incident light and does not experience radiation torque.

The central regions of the Gaussian beam (assumed to be a collimated beam) contribute to the angular alignment. The peripheral regions (away from the beam axis) of the beam contribute to the optical trapping. This is especially so in the axial direction, because a larger gradient force component of optical trapping can be produced. The radial intensity gradient associated with a $TEM_{00}$ Gaussian beam gives rise to a

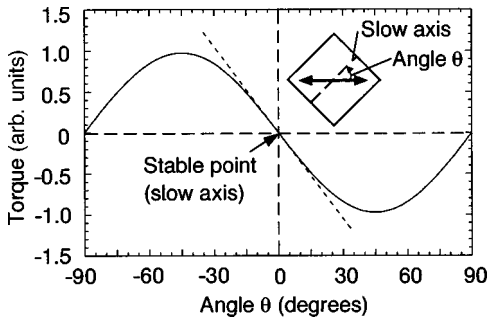


FIG. 2. Calculated radiation torque exerted on the birefringent micro-object (retardation $R=\lambda/4$) as a function of the angle $\theta$ between the slow axis of the birefringent micro-object and incident electric field vector. The inset shows the top view of the birefringent micro-object with the vibration plane of the electric field.

net transverse force, which pulls the micro-object towards the beam axis.

In the case of $R=\lambda/4$, the angular momentum density $\mathbf{J}$ for resultant elliptically polarized light is given by [26,30]

$$\mathbf{J}=\frac{\varepsilon}{2\omega}E_0^2\sin 2\theta\hat{\mathbf{i}}, \tag{1}$$

where $\varepsilon$ is the dielectric permittivity, $\omega$ is the frequency of the light, $E_0$ is the amplitude of the electric field vector, and $\theta$ is the angle of the slow axis of the birefringent micro-object with respect to the vibration plane of the electric field. Thus the radiation torque (the average rate of transport of angular momentum) exerted on the birefringent micro-object changes as $-T_{\max}\sin(2\theta)$, as shown in Fig. 2. As can be seen from this, the maximum torque can be obtained at $\theta=\pm 45°$ where resultant photons are in a pure circularly polarized state and carrying an angular momentum of $\hbar$ per photon. For example, for $\lambda=1.064\,\mu$m, power $P=10$ mW, and $\theta=\pm 45°$, the maximum torque is obtained as $T_{\max}=5.65\times 10^{-18}$ Nm. The torque is proportional to the incident laser power. The resultant elliptically polarized light changes the rotational direction of its electric field depending on the sign of the angle $\theta$ between the vibration plane and the slow axis. A consequent restoring torque exists that draws the slow axis of the micro-object towards the vibration plane. Thus the trapped birefringent micro-object is aligned angularly by interaction between its birefringence and the linearly polarized light. Note that a restoring torque is exerted on the micro-object even at $45°<\theta<90°$ or $-90°<\theta<-45°$, although the magnitude of this torque is small, as shown in Fig. 2.

Furthermore, the linear region around zero degrees can be used for detecting small forces using the optically trapped birefringent micro-object as a new force transducer based on a torsion spring. Indeed, if $\theta(\text{degrees})\ll 90/\pi$, the curve is approximated as $T=-k_\theta\times\theta=-(\pi/90)\times\theta$ (tilted dashed line in Fig. 2). For example, detection of an angle change $\Delta\theta$ of 5 degrees corresponds to a torque change of $9.86\times 10^{-19}$ Nm ($\lambda=1.064\,\mu$m and $P=10$ mW).

Figure 3 shows the experimental setup for optical trapping and angular alignment of birefringent micro-objects. A cw Nd:YAG laser (linear polarization, $\lambda=1.064\,\mu$m, $TEM_{00}$ mode) was used as a trapping light source. The laser beam was expanded and introduced into a conventional optical mi-

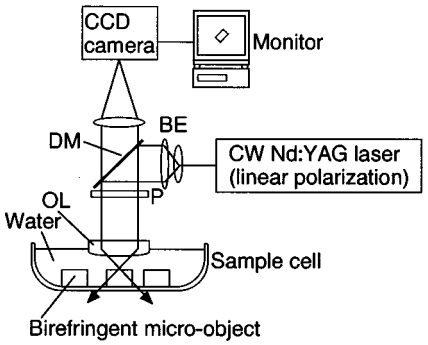


FIG. 3. Experimental setup for optical trapping and angular alignment of the birefringent micro-objects. BE: Beam expander; DM: Dichroic mirror; *P*: λ/2 or λ/4 plate; OL: Objective lens.

croscope (Olympus BH-2). The downward-directed laser beam was focused with a water-immersion objective lens (Olympus LUMPlanFL, 60×, N.A.=0.9, working distance =2.0 mm, infinity-corrected, no cover glass). The beam created an optical trap in a water-filled sample cell mounted on the microscope. A half- or quarter-wave plate placed before the objective lens was rotatable in the horizontal plane to control the state of the polarization. To prevent the polarization state from changing from linear to elliptical at the mirrors, the laser light was incident to all the mirrors in the *s*-polarized state. Micro-objects fabricated by micromachining, as described later, were simply dispersed in water ($n=1.33$). The maximum laser power incident on the micro-objects was 80 mW (measured after the objective lens). The behavior of the trapped micro-objects was observed using a CCD camera system.

We used fluorinated polyimide, PMDA/TFDB [31], as the birefringent material for the micro-objects because of the following advantages. It exhibits high transparency in the near-infrared region and is easy to process. In particular, this polyimide has a rodlike structure accompanied by a large polarizability anisotropy. Thus it has large birefringence ($\Delta n=n_{\mathrm{slow}}-n_{\mathrm{fast}}=1.62-1.49=0.13$ for $\lambda=1.064\,\mu$m) and has been investigated for use in a novel wave plate [32].

To produce micrometer-sized birefringent objects with specific shapes, we used micromachining (photolithography and reactive ion etching). The fabrication procedure had four steps: (i) spin-coating of poly(amic acid) solution onto the silicon (Si) substrate; (ii) curing it at 370 °C in nitrogen; (iii) forming micro-objects by photolithography and reactive ion etching; and (iv) releasing the micro-objects from the substrate and dispersing them water. The thickness of the polyimide film was controlled by changing the spinning speed of the poly(amic acid) solutions and the thickness used in this study was 12 $\mu$m. During curing, the polyimide molecules oriented themselves along the Si substrate. Figure 4 shows the refractive-index ellipsoid of the fluorinated polyimide film on the Si substrate. The polyimide film exhibits a large birefringence ($\Delta n=0.13$) for the $x$ or $y$ propagating light having vibration plane parallel ($n_{\mathrm{slow}}=1.62$) and perpendicular ($n_{\mathrm{fast}}=1.49$) to the film ($x$-$y$) plane, while there is no birefringence for the $z$ propagating light ($n_{\mathrm{slow}}=1.62$). Thus the fluorinated polyimide film behaves as a negative uniaxial crystal with its optical axis perpendicular ($z$ direction) to the

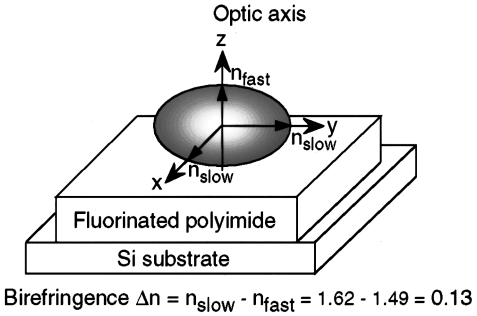


FIG. 4. Schematic illustration (three-dimensional view) of the refractive index ellipsoid of the birefringent fluorinated polyimide on silicon substrate ($\Delta n=n_{\mathrm{slow}}-n_{\mathrm{fast}}=1.62-1.49=0.13$).

Si substrate. Scanning electron micrographs of two fabricated birefringent micro-objects on the Si substrate are shown in Fig. 5.

Micro-objects having three different thicknesses ($d=5$, 10, and 15 $\mu$m) were used in this study to obtain various retardations. These thicknesses correspond to the retardation $R(\Delta n\times d)$ of 0.65 $\mu$m (0.61λ, $\lambda=1.064\,\mu$m), 1.3 $\mu$m (1.22λ), and 1.95 $\mu$m (1.83λ), respectively. We can determine the locations of the fast and slow axes of each micro-object from their designed shapes and dimensions. When we trapped the birefringent micro-objects, the fast and slow axes of the micro-objects did not necessarily direct perpendicular to the propagating laser beam axis in optical traps. To direct these axes perpendicular to the beam axis according to our proposed theory (Fig. 1), we performed the experiments as follows.

(i) When we trapped the micro-objects two-dimensionally (on the bottom of the sample cell), either both axes directed perpendicular or one of the axes (fast or slow) directed parallel to the beam axis. If one axis was along the laser beam axis, we used the trapping beam to manipulate (rotate) the micro-object to direct both axes perpendicular to the beam axis.

(ii) When we trapped the micro-objects three-dimensionally, the locations of these axes depended strongly on the shape of the micro-objects. In general when elongated micro-objects were trapped three-dimensionally, they were aligned with their long dimensions along the beam axis [33]. Therefore, we selectively used only the micro-objects having these axes directed perpendicular to the beam axis when trapped three-dimensionally. These micro-objects generally had short dimensions along the fast and slow axes.

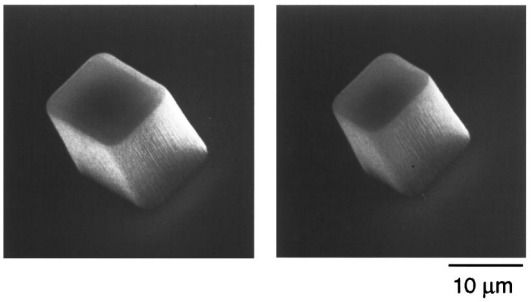


FIG. 5. Scanning electron micrographs of the fabricated birefringent micro-object on the silicon substrate.

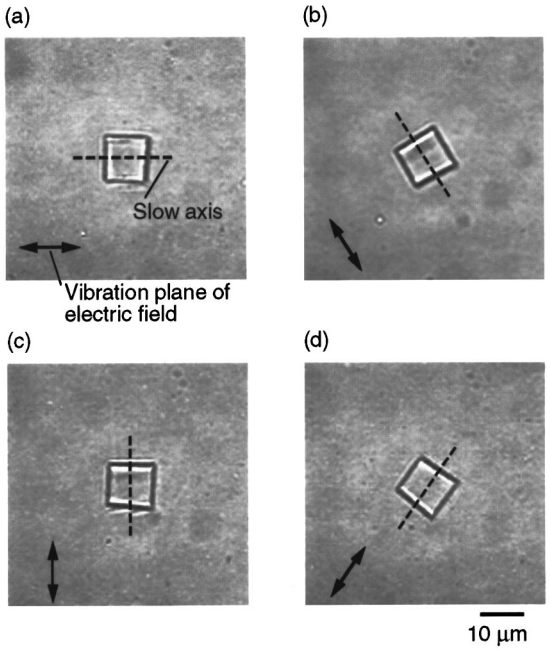


FIG. 6. Micrographs showing the optically induced angular alignment of the birefringent micro-object (thickness: 10 $\mu$m) in water. The direction of the vibration plane of the electric field is shown at the bottom left of each photograph, to indicate the corresponding angular position of the micro-object. The trapping laser beam was irradiated perpendicular to the plane of the photograph and focused around the top surface of the micro-object. The direction of the vibration plane was rotated by 180° [(a)–(d)]. The incident laser power was 10 mW.

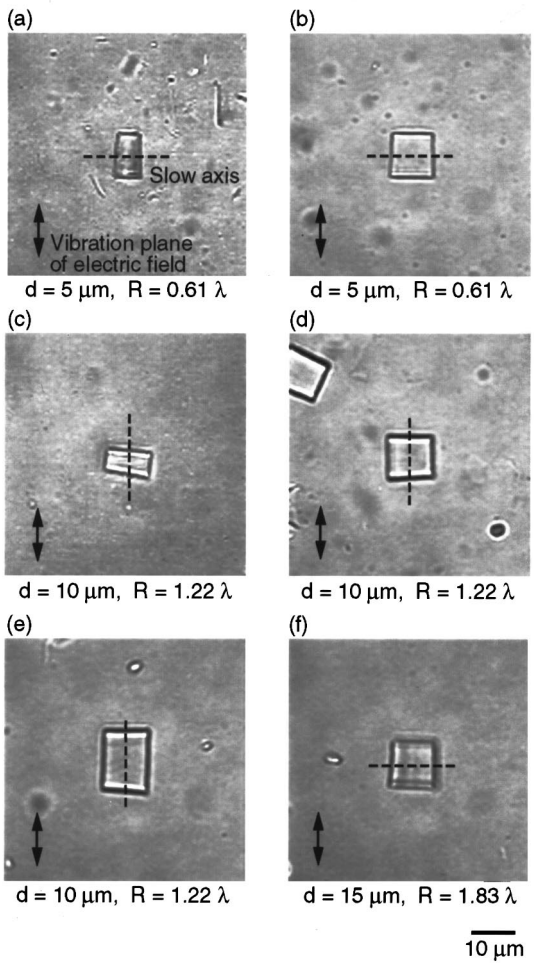


FIG. 7. Micrographs showing the optically induced angular alignment of birefringent micro-objects having different retardations in water. The thicknesses of the micro-objects (in the direction of laser beam propagation) of 5, 10, and 15 $\mu$m correspond to retardations of 0.65 $\mu$m (0.61λ), 1.3 $\mu$m (1.22λ), and 1.95 $\mu$m (1.83λ), respectively. The incident laser power was 10 mW.

Figure 6 shows the optically induced angular alignment of the birefringent micro-objects ($d=10\,\mu$m) in water on the bottom of the sample cell (i.e., a two-dimensional trap) as observed using a linearly polarized laser beam. The trapping laser beam was irradiated perpendicular to the plane of the photograph and focused around the top surface of the micro-object. As soon as the linearly polarized laser beam ($P=10$ mW, polarization ratio: $10^4$:1) was switched on, the micro-object was drawn into the high-intensity region of the laser beam by radiation pressure and itself aligned angularly in the optical trap as shown in Fig. 6(a). When the vibration plane of electric field was rotated by 180° by rotating the λ/2 plate in front of the objective lens (as shown in Fig. 3) by 90°, the micro-object followed the change in direction of the vibration plane within a few seconds [Figs. 6(a)–6(d)]. The micro-object was made to align at arbitrary desired angular positions by changing the direction of the vibration plane. Angular alignment was maintained even at an input power as low as 130 $\mu$W.

We successfully aligned birefringent micro-objects having various retardations as shown in Fig. 7. The micro-object [Fig. 7(f)] having a long dimension in the direction of the laser beam axis was trapped in three dimensions and the other micro-objects were trapped in two dimensions to align their fast and slow axes perpendicular to the laser beam axis. Each trapped micro-object was always aligned in the same direction. Which axis (slow or fast) of the micro-objects coincided with the vibration plane was determined by the retardation of the micro-objects. This is because the rotational direction of the electric field of the resultant elliptically polarized light depended on the retardation of the birefringent micro-object. For birefringent micro-objects having retardation in the range of $\lambda\times m<R<\lambda/2\times(2m+1)$ ($m=0,1,2,...$), e.g., 10-$\mu$m-thick micro-objects in our experiment [Figs. 7(c)–7(e)], the rotational direction of the resultant elliptically polarized light resulted in rightward rotation (as viewed facing into the light) and the slow axis of the birefringent micro-object served as a stable equilibrium axis. Conversely, for birefringent micro-objects having retardation in the range of $\lambda/2\times(2m-1)<R<\lambda\times m$ ($m=1,2,3,...$), e.g., 5- and 15-$\mu$m-thick micro-objects [Figs. 7(a), 7(b), and 7(f)], the rotational direction of the resultant elliptically polarized light resulted in leftward rotation and the fast axis of the micro-object coincided with the vibration plane.

We measured the standard deviation of angular fluctuation of an aligned micro-object. Since the random angular displacement due to Brownian motion (rotation) is significant for small micro-objects [34], we used the smallest micro-object ($d=5\,\mu$m, $R=0.61\lambda$) among our samples for the measurement. The measurements were made by process-

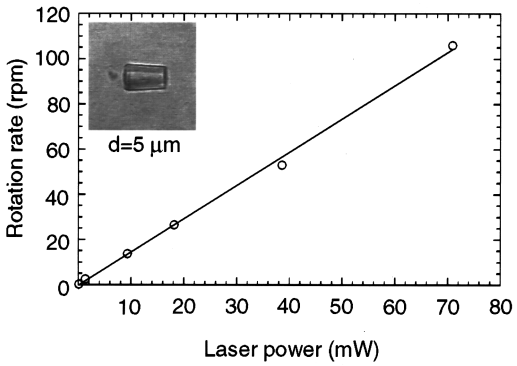


FIG. 8. Laser-power dependence of rotation rate of the birefringent micro-object with circularly polarized light. The inset shows the top view of the trapped birefringent micro-object ($d=5\ \mu$m; $R=0.61\lambda$).

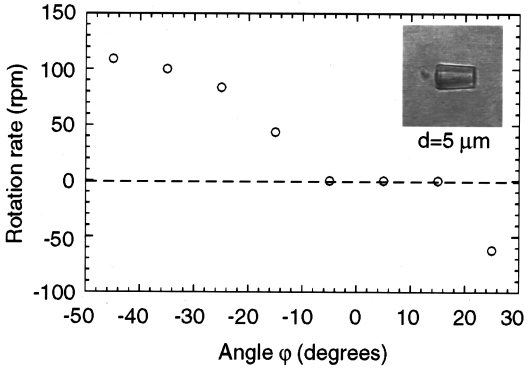


FIG. 9. Rotation rate of the micro-object ($d=5\ \mu$m; $R=0.61\lambda$) as a function of the angle between the vibration plane of the incident electric field and the slow axis of the λ/4 plate located in front of the microscope objective lens (as shown in Fig. 3). This angle represents the degree of ellipticity of the incident beam. The incident laser power was 76 mW.

ing twenty video images taken at three-second intervals. For example, for laser power $P=10$ mW, the standard deviation of angular fluctuation was 1.2°. This value was close to the theoretical value (1.37°) estimated by the equipartition theorem (the thermal energy per degree of freedom is equal to the mechanical energy of the particle, so that $\sqrt{\langle\theta^2\rangle}=\sqrt{k_BT/k_\theta}$, where $k_BT$ is Boltzmann's constant times the absolute temperature). The angular displacement was especially apparent at lower laser power levels, where the restoring radiation torque is small. Adjusting the optimum retardation [the maximum torque can be obtained when using a retardation of $\lambda/4\times(2m+1)$ $(m=0,1,2,...)$] and increasing the laser power should make possible even more accurate angular positioning of the micro-objects.

Next, we investigated the continuous rotation of optically trapped birefringent micro-objects caused by the transfer of the spin angular momentum of a circularly polarized laser beam. By rotating a λ/4 plate inserted in front of the objective lens (as shown in Fig. 3), we easily controlled and observed clockwise rotation, zero rotation (for linear polarization), and counterclockwise rotation, depending on the handedness of the ellipticity. Figure 8 shows the linear relationship observed between input laser power (measured after the objective lens) and rotation rate of the birefringent micro-object ($d=5\ \mu$m, $R=0.61\lambda$). Continuous rotation was observed even at a laser power as low as 0.12 mW.

The radiation torque resulting from the transfer of the spin angular momentum of a circularly polarized light is a function of the retardation and can be expressed as $T=T_{\max}\sin^2(180\times R/\lambda)$ [12,26]. The maximum radiation torque $T_{\max}=2P/\omega$, where $\omega$ is the frequency of the light, can be obtained when using a micro-object having retardation of $\lambda/2\times(2m+1)$ $(m=0,1,2,...)$ in which the direction of the forward transmitted light is completely reversed from that of the incident light. Thus the radiation torque exerted on the micro-object having $R=0.61\lambda$ is estimated as $0.885\times T_{\max}$. For $P=38.6$ mW, we obtain $T_{R=0.61}=3.9\times10^{-17}$ Nm.

Figure 9 shows the rotation rate of the micro-object ($d=5\ \mu$m, $R=0.61\lambda$) as a function of the angle $\varphi$ between the vibration plane of incident light and the slow axis of the λ/4 plate inserted in front of the objective lens (as shown in Fig. 3). This angle $\varphi$ represents the degree of ellipticity of the incident beam. In this case both alignment torque from the linearly polarized component and continuous-rotation torque from the circularly polarized components exerted on the micro-object. This torque can be expressed as [26]

$$T_{\text{alignment}}=-\frac{P}{\omega}\sin\left(360\times\frac{R}{\lambda}\right)\cos(2\varphi)\sin(2\theta), \tag{2}$$

$$T_{\text{rotation}}=\frac{2P}{\omega}\sin^2\left(180\times\frac{R}{\lambda}\right)\sin(2\varphi). \tag{3}$$

The rotation was zero around an angle of zero degrees. (The incident light was elliptically polarized light having an almost linearly polarized component.) This is because the continuous-rotation torque ($T_{\text{rotation}}$) from the circularly polarized component did not exceed the alignment torque ($T_{\text{alignment}}$) from the linearly polarized component. The theoretical value of this threshold angle $\varphi$ is ±9.9° ($R=0.61\lambda$). This result is consistent with results by Friese *et al.* [26].

Using birefringent micro-objects for continuous rotation, due to the transfer of spin angular momentum, has some advantages compared to using absorbing particles: (i) three-dimensional trapping can be easily achieved; (ii) a maximum torque of $2\hbar$ per photon caused by the spin angular momentum can be transferred to the object, compared with $\hbar$ per photon for absorbing particles; and (iii) incident power can be increased significantly when using a transparent birefringent material, while absorption gives rise to heating and can damage absorbing spheres and produce photophoretic forces on them.

In conclusion, we have experimentally demonstrated optically induced angular alignment of trapped birefringent micromachined objects ($\Delta n=0.13$). This angular alignment is caused by the transfer of angular momentum produced by birefringence to the micro-object when linearly polarized incident light is used. We have shown that the retardation of the birefringent micro-object determines which axis (slow or

fast) of the micro-object coincides with the vibration plane of the electric field of the incident light. We expect this direct mechanical effect of optical angular alignment to be useful for micro-opto-mechanical systems, such as for orientation and assembly of micro-optical components in the future. In biological applications, it should be possible to use an optically trapped birefringent micro-object as a torsion spring in a sensing probe for studying biological mechanics.


[1] A. Ashkin, Phys. Rev. Lett. **24**, 156 (1970).

[2] A. Ashkin, J. M. Dziedzic, J. E. Bjorkholm, and S. Chu, Opt. Lett. **11**, 288 (1986).

[3] A. Ashkin, Proc. Natl. Acad. Sci. USA **94**, 4853 (1997).

[4] E. Higurashi, H. Ukita, H. Tanaka, and O. Ohguchi, Appl. Phys. Lett. **64**, 2209 (1994).

[5] E. Higurashi, H. Ukita, H. Tanaka, and O. Ohguchi, *Proceedings of IEEE Micro Electro Mechanical Systems*, Oiso, Japan (IEEE, New York, 1994), p. 291.

[6] R. C. Gauthier, Appl. Phys. Lett. **67**, 2269 (1995).

[7] Y. Ohmachi, K. Baba, and E. Higurashi, Proc. SPIE **2882**, 333 (1996).

[8] R. C. Gauthier, Appl. Phys. Lett. **69**, 2015 (1996).

[9] E. Higurashi, O. Ohguchi, T. Tamamura, H. Ukita, and R. Sawada, J. Appl. Phys. **82**, 2773 (1997).

[10] H. Ukita and K. Nagatomi, Opt. Rev. **4**, 447 (1997).

[11] E. Higurashi, R. Sawada, and T. Ito, Appl. Phys. Lett. **72**, 2951 (1998).

[12] R. A. Beth, Phys. Rev. **50**, 115 (1936).

[13] L. Allen, M. W. Beijersbergen, R. J. C. Spreeuw, and J. P. Woerdman, Phys. Rev. A **45**, 8185 (1992).

[14] A. Ashkin and J. M. Dziedzic, Appl. Phys. Lett. **28**, 333 (1976).

[15] T. Sugiura, S. Kawata, and S. Minami, J. Spectrosc. Soc. Jpn. **39**, 342 (1990) (in Japanese).

[16] H. He, M. E. J. Friese, N. R. Heckenberg, and H. Rubinsztein-Dunlop, Phys. Rev. Lett. **75**, 826 (1995).

[17] H. He, N. R. Heckenberg, and H. Rubinsztein-Dunlop, J. Mod. Opt. **42**, 217 (1995).

[18] M. E. J. Friese, J. Enger, H. Rubinsztein-Dunlop, and N. R. Heckenberg, Phys. Rev. A **54**, 1593 (1996).

[19] N. B. Simpson, L. Allen, and M. J. Padgett, J. Mod. Opt. **43**, 2485 (1996).

[20] N. B. Simpson, K. Dholakia, L. Allen, and M. J. Padgett, Opt. Lett. **22**, 52 (1997).

[21] M. E. J. Friese, T. A. Nieminen, N. R. Heckenberg, and H. Rubinsztein-Dunlop, Opt. Lett. **23**, 1 (1998).

[22] P. L. Marston and J. H. Crichton, Phys. Rev. A **30**, 2508 (1984).

[23] S. Chang and S. S. Lee, J. Opt. Soc. Am. B **2**, 1853 (1985).

[24] J. P. Barton, D. R. Alexander, and S. A. Schaub, J. Appl. Phys. **66**, 4594 (1989).

[25] E. Higurashi, R. Sawada, and T. Ito, Technical Digest of IEEE/LEOS IEEJ/SAMS International Conference on Optical MEMS and Their Applications MOEMS'97, Nara, Japan (1997), p. 186 (unpublished).

[26] M. E. J. Friese, T. A. Nieminen, N. R. Heckenberg, and H. Rubinsztein-Dunlop, Nature (London) **394**, 348 (1998).

[27] P. J. Allen, Am. J. Phys. **74**, 1185 (1966).

[28] G. G. Padmabandu and A. S. Marathay, Opt. Eng. (Bellingham) **31**, 1342 (1992).

[29] E. Santamoto, B. Daino, M. Romagnoli, M. Settemlre, and Y. R. Shen, Phys. Rev. Lett. **57**, 2433 (1986).

[30] S. M. Barnett and L. Allen, Opt. Commun. **110**, 670 (1994).

[31] T. Matsuura, S. Ando, S. Sasaki, and F. Yamamoto, Macromolecules **27**, 6665 (1994).

[32] S. Ando, T. Sawada, and Y. Inoue, Electron. Lett. **29**, 2143 (1993).

[33] R. C. Gauthier, J. Opt. Soc. Am. B **14**, 3323 (1997).

[34] A. Einstein, in *Theory of the Brownian Movement*, edited by R. Fürth (Dover, New York, 1956).